

Electron transport of a quantum wire containing a finite-size impurity under THz electromagnetic field illumination

Guanghui Zhou^{1,2,3,*}, Yuan Li², Fang Cheng², and Wenfu Liao²

¹CCAST (World Laboratory), PO Box 8730, Beijing 100080, China

²Department of Physics, Hunan Normal University, Changsha 410081, China[†] and

³International Center for Materials Physics, Chinese Academy of Sciences, Shenyang 110015, China

We theoretically investigate the electron transport properties for a semiconductor quantum wire containing a single finite-size attractive impurity under an external terahertz electromagnetic field illumination in the ballistic limit. Within the effective mass free-electron approximation, the scattering matrix for the system has been formulated by means of a time-dependent mode matching method. Some interesting properties of the electron transmission for the system have been shown through a few groups of numerical examples. It is found that in the case of the comparative stronger field amplitude and the frequency resonant with the two lowest lateral energy levels in the impurity region, the field-induced intersubband transition dominates the process as if without the impurity. And there is a step-arising on the transmission as a function of the incident electron energy. However, in the case of lower field amplitude and the non-resonant frequencies both multiple symmetry Breit-type resonance peaks and asymmetry Fano-type dip lines appear in the electron transmission dependence on the incident energy due to the presence of the impurity and the external field. Therefore, within certain energy range the transmission as a function of the field frequency and/or field amplitude shows a rich structure. Moreover, the transmission dependence on the strength and size of the impurity is also discussed. It is suggested that these results mostly arise from the interplay effects between the impurity in a quantum wire and the applied field.

PACS numbers: 73.23.-b; 73.21.Hb; 78.67.Lt

I. INTRODUCTION

Quantum devices using a two-dimensional electron gas (2DEG) formed in high-mobility GaAs/Al_xGa_{1-x}As semiconductor heterostructure have been found to have better performance characteristics than bulk devices. It has been predicated that the characteristics of the devices may be further improved by using quantum wires in which the carriers behave as a quasi-one-dimensional gas. And some technological success has been achieved in recent years in growing high-quality semiconductor quantum wires with a length up to μm .¹ In the ballistic regime and at low temperatures quantum coherent effects will dominate the electron transport properties of a mesoscopic system. One of the most important features is that, when the lateral size of a quantum wire varies, the conductance shows an histogram structure and each step has an height of $2e^2/h$ or integer times of it for both short wire² (quantum point contact) and long wire.^{1,3}

The electron transport properties of the quantum wire formed on a 2DEG can be affected by many factors. The presence of disorders in a quantum wire generally leads to a suppression of the conductance plateaus below integer values.⁴ Especially, for a quantum wire containing an attractive impurity the transmission shows resonance dips below each confinement subband.⁵⁻⁷ Also, the interaction of electrons induces transport anomalies.⁸ However, there has been growing interest in the time-dependent transport for quantum wire systems in recent years, such as presence of a time-modulated potential⁹ and quantum pumping.¹⁰ Further, when a quantum wire is illuminated under an external electromagnetic (EM) field, due to the inelastic scattering of electrons by photons many new features have been observed experimentally^{11,12} and predicted theoretically.¹³⁻¹⁵ The technique of applying an external field is of particular interest, since no additional current and voltage probes have to be attached to the sample which may disturb the system's properties. More recently, a new type of giant magnetoresistance has been discovered¹⁶ and theoretically explained¹⁷ in a high-mobility 2DEG subject to a high frequency microwave radiation and a vertical magnetic field. It is therefore of great interest in basic physics aspect to study the time-dependent transport properties of quantum structures on semiconductor 2DEG system. On the other hand, possible applications of nanostructures in future electronic devices, which will have to operate at very high frequencies, require detailed knowledge of their frequency- and time-dependent transport behavior.

The values of the lateral energy level separation and the Fermi energy are of the order of 1~100meV for the typical semiconductor quantum wires. This corresponds to frequencies of the range of 0.25~25 terahertz (THz), which is

[†] Mailing address

available in experiments with the development of the ultrafast laser technology and the physics in this frequency range is of interest now.¹⁸ When the Fermi level is below the lowest lateral level at the bottleneck part of a quantum wire, electrons can not go through without the assistance of an external EM field. However, under the field illumination, electrons in the wire can absorb energy of photons and go through this geometric barrier (the neck). Therefore, in the region of barrier the electron transmission is determined by the combined effect of the external EM field and the wire lateral shape variation.^{11–14} Recently, with an emphasis on the pure EM field effect on the electron transport, we have theoretically investigated¹⁹ a straight (uniform cross-section) and clean (without impurity) quantum wire illuminated under a transversely polarized THz EM field. An interesting transmission step-like structure has been predicated when the EM field frequency is resonant with the two lowest lateral energy levels of the quantum wire. Also, the impurity effect on the transport is important for a thin and long quantum wire because the electron interaction effect is observable in the presence of backscattering.^{1,3} Without considering this interaction, the resonance structures of the electron transmission in a straight quantum wire with a finite-size scatter for a wide range of the impurity parameters have been investigated in the absence of external EM field.⁷ In the present paper, we combine the models in Refs.[7,19] and study the electron transmission through a straight quantum wire containing a finite-size attractive impurity under a transversely polarized THz EM field illumination. In this case the transmission behavior may reflect the interplay effects between the impurity⁷ and the external EM field¹⁹ on the electron transport. Within the effective mass free-electron approximation, the scattering matrix for the system has been formulated through a time-dependent mode matching method.¹⁹ Using a group of numerical examples we demonstrate some interesting electron transmission behaviors for this system. To the best of our knowledge, the interplay effect between the impurity and the external EM field on the electron transport for a quantum wire has not been reported previously. This effect may be important for the understanding of basic physics in low-dimensional systems and for the future nanoscale circuit applications.

The outline of the paper is as follows. In Sec. II we set up the problem for a straight quantum wire containing a finite-size impurity under an external THz EM field illumination in terms of a single-electron time-dependent Schrödinger equation, and calculate the electron transmission probability through the system by the time-dependent mode matching in the framework of Landauer-Büttiker formalism. Some numerical examples to illustrate the dependence of the electron transmission on the incident energy, field parameters, and impurity parameters respectively are presented and discussed in Sec. III. Finally, Sec. IV gives a conclusion of the paper.

II. MODEL AND FORMALISM

The system under study is an ideal straight 2D quantum wire (quantum waveguide) of width D , containing a finite-size attractive impurity, which is depicted in Fig. 1 schematically.^{7,19} The quantum wire smoothly connects the two electron reservoirs (leads) at each end. The x-axis is longitudinally along the wire, and the y-axis describes the transverse direction. The impurity range $0 \leq x \leq l$ in the quantum wire is illuminated under a transversely polarized THz EM field in an unspecified way. The field vector potential can be described as $\mathbf{A} = (\varepsilon/\omega) \cos(\omega t) \hat{e}_y$ with angular frequency ω and amplitude ε (\hat{e}_y is the unit vector in the polarized direction).

Within an effective mass approximation, the single-particle time-dependent Schrödinger equation in the field illuminated impurity region is

$$i \frac{\partial}{\partial t} \Psi(x, y, t) = \left[-\frac{\partial^2}{\partial x^2} + (-i \frac{\partial}{\partial y} + eA)^2 + v_c(y) + v_i(x, y) \right] \Psi(x, y, t), \quad (1)$$

where we have adopted the unit of $\hbar = 2m^* = 1$. In the Hamiltonian, $v_c(y)$ presents a transverse confining potential in the form of either a hard-wall or parabolic one which confines electrons to the wire and to the reservoirs, and

$$v_i(x, y) = \theta(x)\theta(l-x)v_i(y) = -v\theta(x)\theta(l-x)\theta(d/2 - |y - y_c|) \quad (2)$$

is used to represent the single finite-size impurity potential, where v is the strength of the impurity and $\theta(x)$ is the step function (see Fig.1). This type of the finite-size single impurity has been used to model an unintentional Be doping in GaAs semiconductor⁵ and may be artificially created in the quantum waveguide using recent nanotechnology.⁶

Using the method used in Ref.[19] (also see Ref.[20]) to solve the time-dependent Schrödinger equation (1), and then considering the scattering of the two interfaces between the impurity region (with field illumination) and the clean region (without field illumination) separately.²¹ The detail knowledge about this aspects is referred to Refs.[19,20] and is not presented here.

When an electron with total incident energy E emits from the left reservoir to the left interface at $x = 0$, transmission and reflection will take place simultaneously. Because the electron has certain probability of absorbing a photon after penetrate the interface, transition from the lower mode to the upper mode happens. So there are two energy

components of E and $E + \hbar\omega$ in the reflected wave in the region of $x < 0$

$$\Psi(x, y, t) = [e^{i(k_1x - Et)} + c_1 e^{-i(k_1x + Et)}] \phi_1(y) + c_2 e^{-i[k_2x + (E + \omega)t]} \phi_2(y), \quad (3)$$

where $\phi_n(y)$ ($n=1,2$) are transverse eigenfunctions with eigenvalues ϵ_n in the clean region (without impurity), c_1, c_2 are the reflection coefficients of the two modes respectively, and

$$k_1 = \sqrt{E - \epsilon_1}, \quad k_2 = \sqrt{E - \epsilon_2 + \omega} \quad (4)$$

are their associated wavevectors. Consequently, we can obtain the electronic wavefunction in the region of $x > 0$

$$\Psi(x, y, t) = [c_+ e^{i(k_+x - Et)} + c_- e^{i(k_-x - Et)}] \psi_1(y) + [G_+ c_+ e^{i[k_+x - (E + \omega)t]} + G_- c_- e^{i[k_-x - (E + \omega)t]}] \psi_2(y), \quad (5)$$

where $\psi_n(y)$ and ϵ'_n are the solutions for the transverse equation with impurity potential $v_i(y)$. c_+, c_- are the transmission coefficients of the two field-split modes and the constants $G_{\pm} = \pm(\sqrt{\gamma^2 + \xi^2} \mp \gamma)/\xi$ (where $\gamma = \omega - (\epsilon'_2 - \epsilon'_1)$ is the detuning, and ξ is the two-mode coupling constant). The two electron wavevectors in the impurity region are

$$k_{\pm} = \sqrt{E - \epsilon'_1 + \gamma/2 \mp \sqrt{\gamma^2 + \xi^2}/2}. \quad (6)$$

We can match the above two wavefunctions (3) and (5) at the interface of $x = 0$. Continuously connecting the two above wavefunctions and their differentials gives the following four algebraical equations for the coefficients c_1, c_2, c_+ and c_-

$$\begin{aligned} \lambda_{11}(1 + c_1) &= c_+ + c_-, \\ \lambda_{22}c_2 &= c_+G_+ + c_-G_-, \\ \lambda_{11}(k_1 - c_1k_2) &= c_+k_+ + c_-k_-, \\ -\lambda_{22}c_2k_2 &= c_+G_+k_+ + c_-G_-k_-, \end{aligned} \quad (7)$$

where $\lambda_{nn'} = \int_{-D/2}^{D/2} dy \psi_n^*(y) \phi_{n'}(y)$ ($n, n' = 1, 2$) is the matrix elements for connecting the two sets of transverse eigenfunctions. With the solution of these algebraic equations in Eq. (7) both the transmission and the reflection matrix for the left interface (as if without the right interface) can be expressed by

$$t' = \begin{bmatrix} \sqrt{k_+/k_1} c_+ & 0 \\ \sqrt{k_-/k_1} c_- & 0 \end{bmatrix}, \quad r = \begin{bmatrix} c_1 & 0 \\ \sqrt{k_2/k_1} c_2 & 0 \end{bmatrix}. \quad (8)$$

When we consider the electron transmission probability through the whole real impurity, we use the approach recently developed in Ref. [21] for the symmetric system. This approach needs to derive the total scattering matrix which can be expressed in the transmission matrix and reflection matrix on each interface. The total transmission matrix is just the anti-diagonal submatrix of the total scattering matrix in the symmetry system case.

Because of the similarity of the two interfaces one has not to match the wave functions at the right interface $x = l$, but we need to know the transmission and reflection matrix of electron emitting from right to left for the left interface. In this case the electronic wavefunction in the impurity region is

$$\begin{aligned} \Psi(x, y, t) &= [c_+^e e^{-ik_+x} + c_+^e e^{-ik_-x} + c_+^r e^{ik_+x} + c_-^r e^{ik_-x}] e^{-iEt} \psi_1(y) \\ &+ [G_+ c_+^e e^{-ik_+x} + G_- c_+^e e^{-ik_-x} + G_+ c_+^r e^{ik_+x} + G_- c_-^r e^{ik_-x}] e^{-i(E + \omega)t} \psi_2(y), \end{aligned} \quad (9)$$

where c_{\pm}^e are the coefficients of the electron emitting from right to left, c_{\pm}^r are the associated reflection coefficients. Correspondingly, the transmitted electron wavefunction in the region of $x < 0$ is

$$\Psi(x, y, t) = c_1^t e^{-i(k_1x + Et)} \phi_1(y) + c_2^t e^{-i[k_2x + (E + \omega)t]} \phi_2(y), \quad (10)$$

where c_1^t and c_2^t are the transmission coefficients. These two wavefunctions also satisfy the continuous condition at $x = 0$, from which we can obtain the transmission and reflection matrix from right to left for this interface, r' and t , respectively (Here we do not present the detailed expressions for them because they are much more complicated than Eq. (8) for t' and r). Consequently, the total transmission matrix through the two interfaces (the whole system) is $t_{tot} = S_{12} = t(1 - Xr'Xr')^{-1}Xt'$. Therefore, according to Landauer-Büttiker's formulation²² the total electron transmission probability through the whole system is

$$T = Tr[t_{tot}^\dagger t_{tot}], \quad (11)$$

where X is the transfer matrix between the two interfaces of the system.¹⁹

III. RESULTS AND DISCUSSION

In this section, we numerically calculate the transmission probability from Eq. (12). The physical quantities of the system are chosen to be a high mobility GaAs/Al_xGa_{1-x}As heterostructure^{1,2} with a typical electron density $n = 2.5 \times 10^{11} \text{cm}^{-2}$ and $m^* = 0.067 m_e$ (where m_e is the free electron mass). We choose the hard-wall transverse confining potential and the width of the wire $D = 500 \text{\AA}$ (see Fig. 1) such that the unit of energy $E^* = \epsilon_1 = \hbar^2 \pi^2 / (2m^* D^2) = 14.1 \text{meV}$ which corresponds to the unit of time $t^* = \hbar / E^* = 4.7 \times 10^{-14} \text{s}$. Correspondingly, the field frequency unit $\omega^* = 1/t^* = 21.3 \text{THz}$ and the amplitude unit $\varepsilon^* = 22.1 \text{V/cm}$. This kind of radiation is available in experiments now.¹⁸ We also use the length unit $l^* = D/\pi = 63.7 \text{\AA}$.

For the hard-wall confining potential with a finite-size impurity of $d = 0.1D$, $l = 25$, $y_c = 0.17D$ (see Fig. 1) and strength $v = 6.3\epsilon_1$, the transverse eigenvalues in the impurity region are solved by the quantum perturbation method as

$$\epsilon'_1 = -0.23\epsilon_1, \quad \epsilon'_2 = 3.34\epsilon_1 \quad (12)$$

with associated eigenfunctions $\psi_1(y) = 0.951\phi_1(y) - 0.314\phi_2(y)$ and $\psi_2(y) = 0.314\phi_1(y) + 0.951\phi_2(y)$. And different transverse eigenvalues as well as eigenfunctions can be obtained by variation of the impurity size.

In the following we systematically present some numerical examples, while restrict our attention to the energy range (ϵ_1, ϵ_2) throughout the work.

A. The characteristics of transmission dependence on incident energy

First of all, in the absence of the EM field, the transmission probability T as a function of incident energy E should be the same as that in Ref. [7], which shows the Breit-Wigner resonances in the lower energies $\epsilon_1 < E < \epsilon'_2$ and the multiple asymmetric Fano lines in the upper energies $\epsilon'_2 < E < \epsilon_2$.

In the presence of the EM field, we show the calculated T versus E for two combinations of the field parameters in Fig. 2 with impurity size of $d = 0.1D$, $l = 25$, $y_c = 0.17D$ and strength $v = 6.37$. The dashed line presents the case of resonant field frequency $\omega = 3.57 (\gamma = 0, \omega = \epsilon'_2 - \epsilon'_1)$ with $\varepsilon = 9.96$, while the solid line gives a representative case of nonresonant frequency $\omega = 2 (\gamma \neq 0)$ with $\varepsilon = 2.97$. In the case of the field frequency resonant (matching) with the energy spacing of the two lowest levels, the transmission probability is similar to that for the case of absent impurity¹⁹ except for a suppression of average 0.1. Also a step-raising of transmission occurs at energy $E = \epsilon'_1 + \xi/2 = 2.52$ (for these field parameters the mode coupling constant $\xi = 5.5$).²³ This interesting phenomenon can be similarly explained by the field-induced intersubband transition.¹⁹ When an electron penetrate through the interface, the transverse levels of the electron in the field illuminated region are dressed and one electron mode is split into the two time-dependent modes with the longitudinal momentum k_+ and k_- , respectively. When $E < \epsilon'_1 + \xi/2$, k_+ is imaginary and its corresponding mode is an evanescent (nonpropagating) mode which contributes nothing to the transmission so that the total transmission probability is suppressed to an half value. Further, when $E > \epsilon'_1 + \xi/2$ the both modes become propagating and all contribute to the transmission. However, with the non-resonant field frequency the structure of transmission probability is much different from the case without impurity. For this case of non-resonant frequency and weaker field amplitude we note that an interesting asymmetry Fano-type resonance dip appear at $E \approx 2$, which indicates the formation of a quasibound states.⁷ Electrons with this particular incident energy can make a transition from a propagating state to a quasibound state by emitting an energy of $\hbar\omega$. So this resonance dip may be a result from the feature of the impurity-induced quasibound state. We can also explain this phenomenon with the mode propagational property. Around the point of $E \sim 2$, from Eqs. (4) and (6) we find that the wavevector $k_2 \sim 0$ and the field-split electron wavevector $k_+ \sim 0$. This indicates that the two modes k_2 and k_+ may be nonpropagating. So that T reaches a nonzero minimum because k_1 and k_- are always propagating.

We also note that there are some resonance oscillations on the two transmission curves in Fig.2. These oscillations physically result from the interference of the forward- and backward-going electron waves induced by the two interfaces of the impurity along the transport direction. The resonance peaks with prefect transmission on the solid line of Fig. 2 appeared at lower energies $E \approx 1.01, 1.39$ and 1.85 may be identified to the symmetry Breit-type resonance and the half width of each resonance specifies the lifetime of the corresponding quasibound state. Therefore, the above characteristics of T dependence on E for the system have implied the differences in electron transmission between the two cases of with and without⁷ EM field and also between the two cases of with and without¹⁹ impurity.

B. Transmission dependence on the field parameters

Next, in this subsection we investigate the influence of the field parameters on the electron transmission with the interesting energy of $E = 2$ for the nonresonant frequency case (see Fig. 2). We present the numerically calculated T as a function of ω and ε as shown in Fig. 3 with the same impurity parameters as that in Fig. 2. From Fig. 3 we can see that the transmission probability T changes between 0 (black) and 1 (white) with the variation of the field parameters and shows several dip structures (black areas) around $\omega \sim 2$, which includes the dip of the solid line in Fig. 2 at $\varepsilon \sim 3$. We also note that there exist perfect transmission areas (complete white). In the region of small ε (regardless of the value of ω) the field is too weak to affect the transmission, while in the region of $\omega > 3.57$ (resonant) regardless of the value of ε the field-induced intersubband transition dominates. However, with the proper combinations of ε and ω perfect transmission also occurs. This interesting phenomenon of perfect and blocked transmission has also been predicted¹⁴ for a narrow-wide-narrow shape clean quantum wire under a EM field illumination for certain combinations of the field parameters.

In the following, we discuss the effects of ω and ε on T separately. Fig.4 shows the calculated T as function of ω for four different values of ε with the same impurity parameters as that in Fig.2. In the case of a rather weak field amplitude $\varepsilon = 1.5$ as shown in Fig. 4(a), multiple Fano resonance lines appear within $\omega = 1.69 \sim 1.82$. This result is very similar to that in Ref.[7] but within the range of higher energies. From Eqs. (4) and (6), we know that in this case mode k_+ begins to open (propagating) earlier than k_2 with $\omega \approx 1.69$ and $\varepsilon = 1.5$ ($\xi = 1.75$). There are two propagating modes (k_+ and k_-) in the impurity region but only k_1 is propagational outside the impurity. The multiple Fano resonances are connected with the interaction of multiple quasidonor levels but lowered by the EM field. In Fig. 4(b) with $\varepsilon = 2.97$ (same value as that in solid line of Fig. 2) there is only one Fano dip at $\omega = 2$, which corresponds to the single dip of the solid line in Fig. 2. Furthermore, as shown in Fig. 4(c) with stronger amplitude $\varepsilon = 6$, T is suppressed with no dip in the range of $2.2 < \omega < 3$ because the open of k_2 enhances the probability of reflection. And T increases when $\omega > 3$ due to the second mode k_+ beginning to be propagating. So it is reasonable when only one mode (k_-) in the illuminated region with $\varepsilon = 10$ is propagating and T is more suppressed as shown in Fig. 4(d).

On the other hand, in Fig. 5 we present the calculated T as function of ε for four different values of ω with the same impurity parameters. For a rather small $\omega = 1$ in Fig. 5(a) T shows an oscillation behavior with almost periodic maximum (perfect transmission) and declined minimum (valley) as ε increases. The oscillation results from the interference of the forward- and backward-going electron waves induced by the two interfaces of the impurity along the transport direction. With a fixed $\omega = 2$, the multiple Fano resonance lines appear as shown in Fig. 5(b) within $\varepsilon = 0.8 \sim 2.6$. The pattern of T is slightly different from that of Fig. 4(a) but with the same physical reason. The perfect transmissions are seen to occur at $\varepsilon=0.78, 1.4, 1.68$ and 2.3 and the asymmetric Fano dips are seen to occur at $\varepsilon=0.8, 1.38, 1.82 \dots$. The second mode (k_+) is the evanescent mode and the coupling of the two modes in field region vanishes as well as the formation of the quasibound states when $\varepsilon > 2.97$ holds. From the above analysis it seems reasonable that the step structure appears around $\varepsilon = 3.4$ in Fig. 5(c) with $\omega = 2.3$. This results from the suppression of the second mode (k_+) with increasing of ε when $\omega > 2$ holds. In Fig. 5(d) with $\omega = 4$ the average T is much enhanced with no dip or step structures because both k_+ and k_2 are propagating modes.

In general for a fixed electron incident energy, a different combination of the field parameters results in a different transmission dependence. But for the chosen geometrical parameters in this work the rich structure of the transmission always appear in the ranges of $E \sim 2$, $\omega \sim 1.5 - 2$ and $\varepsilon \sim 1 - 3$.

C. Transmission dependence on the impurity parameters

Finally, in this subsection we investigate the effects of the impurity parameters on the transmission probability T for the same system.

We first consider the effect of impurity size on the transmission. An example of different impurity width $d = 0.2D$ has been adopted and its corresponding transverse eigenvalues have been calculated as $\epsilon'_1 = -1.85$ and $\epsilon'_2 = 3.19$. Fig. 6 shows the numerical results of T as a function of E with a fixed $\omega = 2$ for two different ε . With $\varepsilon = 2.97$ the multiple Fano resonances appear in Fig. 6(a) within a energy range of $E = 1.6 \sim 1.8$. However, Fig. 6(b) shows that as ε increases to 3.6 with the same ω , a single Fano dip line (similar to the solid line in Fig. 2) appears. This indicates that the two modes (k_2 and k_+) begin to be propagating. Comparing with the solid line in Fig. 2 we conclude that as the width of the impurity increases, it need stronger field amplitude ε to suppress the splitting of the second mode. But this conclusion may not be extended to the increase of length l .

Next, we consider the effect of the impurity strength on the transmission. An example of different impurity strength of $v = 8.0\epsilon_1$ has been adopted and its associated eigenvalues have been recalculated as $\epsilon'_1 = -0.64$ and $\epsilon'_2 = 3.26$. Fig. 7 shows the numerical results of T as a function of E with a fixed $\omega = 2$ for two different ε . A asymmetry Fano dip

also occurs in Fig. 7(a) at $E \approx 1.9$ (with $\varepsilon = 2.97$) and in Fig. 7(b) at $E \approx 2$ (with $\varepsilon = 3.2$). From this result we conclude that with the same ω although the increase of the impurity strength one need stronger field amplitude ε to suppress the splitting of the second mode. It seems that the variation of the impurity strength does not change the transmission behavior much even if we use a δ potential to model the impurity. And this fact of model independence is physically reasonable.

IV. CONCLUSION

We have theoretically investigated the electron transport properties for a straight semiconductor quantum wire containing a single finite-size attractive impurity under a THz EM field illumination in the ballistic limit. Within the effective free-electron approximation, a single-particle time-dependent Schrödinger equation was established and the scattering matrix for the system was formulated via the method of time-dependent mode matching.

The numerical examples predicate that a step-arising on the transmission probability versus the electron incident energy occurs in the case of the field frequency resonant with the lateral energy spacing of the two lowest levels. This situation is similar to the case of the system without¹⁹ impurity and the physical origin is mainly the coherent field-induced intersubband transition. However, due to the interplay between the impurity-induced quasibound states and the applied field, both multiple symmetry Breit-type resonance peaks and asymmetry Fan-type dip lines appear within the energy range of $(\varepsilon_1, \varepsilon_2)$ in the case of a weaker field amplitude and the non-resonant field frequency. This situation is also consistent with the system⁷ without field illumination. Further, the dependence of the transmission on either field amplitude or frequency also indicates the change of the shape and the position of the resonance dips. But the rich structure of the transmission always appears with the proper combination of the field parameters. Moreover, the transmission behavior is almost independent on the impurity parameters.

Therefore, from the results of this work we conclude that the field parameters ω and ε can control the characteristics of electron transmission through the propagational property of the modes in a quantum wire. These effects of the applied field on the transport properties in a quantum wire may be useful for understanding basic physics of quantum structures and for device physics.

Acknowledgments

This work was supported by the Nature Science Foundation of Hunan (NO. 02JJY2008) and by the Research Foundation of Hunan Education Commission (NO. 04A031).

-
- * Electronic address: ghzhou@hunnu.edu.cn
- ¹ A. Yacoby, H.L. Stormer, N.S. Wingreen, L.N. Pfeiffer, K.W. Baldwin, and K.W. West, Phys. Rev. Lett. **77**, 4612 (1996); C.T. Liang, M. Pepper, M.Y. Simmons, C.G. Smith, and D.A. Ritchie, Phys. Rev. **B61**, 9952 (2000); R. de Picciotto, L.N. Pfeiffer, K.W. Baldwin, and K.W. West, Phys. Rev. Lett. **92**, 36805 (2004).
 - ² B.J. van Wees, H. van Houten, C.W.J. Beenakker, J. G. Williamson, L.P. Kouwenhoven, D. van der Marel, and C.T. Foxon, Phys. Rev. Lett. **60**, 848 (1988); D.A. Wharam, T.J. Thornton, R. Newbury, M. Pepper, H. Ahmed, J.E.F. Frost, D.G. Hasko, D.C. Peacock, D.A. Ritchie, and G.A.C. Jones, J. Phys. **C21**, L209 (1988).
 - ³ A. Szafer and A.D. Stone, Phys. Rev. Lett. **62**, 300 (1989); D.L. Maslov and M. Stone, Phys. Rev. **B52**, R5539 (1995).
 - ⁴ D. Boese, M. Lischka, and L.E. Reichl, Phys. Rev. **B62**, 16933 (2000).
 - ⁵ C.S. Chu and R.S. Sorbello, Phys. Rev. **B40**, 5941 (1989); A. Kumar and P.F. Bagwell, Phys. Rev. **B43**, 9012 (1991); S.A. Gurvitz and Y.B. Levinson, Phys. Rev. **B47**, 10578 (1993).
 - ⁶ Y.S. Joe and R.M. Cosby, J. Appl. Phys. **81**, 6217 (1997); S. Yamada and M. Yamamoto, J. Appl. Phys. **79**, 8391 (1996).
 - ⁷ Chang Sub Kim, Arkady M. Satanin, Yong S. Joe, and Ronald M. Cosby, Phys. Rev. **B60**, 10962 (1999).
 - ⁸ M. Ogata and H. Fukuyama, Phys. Rev. Lett. **73**, 468 (1994); O.P. Sushkov, Phys. Rev. **B64**, 155319 (2001).
 - ⁹ Qing-feng Sun, Jian Wang, and Tsung-han Lin, Phys. Rev. **B60**, R13981 (1999); M.L. Maslov, Phys. Rev. **B52**, R14368 (1995); C.S. Tang, Y.H. Tan, and C.S. Chu, Phys. Rev. **B67**, 205324 (2003).
 - ¹⁰ P. W. Brouwer, Phys. Rev. **B58** R10135 (1998); E.R. Mucciolo, C. Chamon, and C.M. Marcus, Phys. Rev. Lett. **89**, 146802 (2002).
 - ¹¹ Q. Hu, Appl. Phys. Lett. **62**, 837 (1993); Shechao Feng and Qing Hu, Phys. Rev. **B48**, 5354 (1993).
 - ¹² D.D. Arnone, J.E.F. Frost, C.G. Smith, D.A. Ritchie, G.A.C. Jones, R.J. Butcher, and M. Pepper, Appl. Phys. Lett. **66**, 3149 (1995).
 - ¹³ O. Tageman, L.Y. Gorelik, R.I. Shekter, and M. Jonson, J. Appl. Phys. **81**, 285 (1997); O. Tageman and A.P. Singh, Phys. Rev. **B60**, 15937 (1999).

- ¹⁴ S. Blom and L.Y. Gorelik, Phys. Rev. B**64**, 45320 (2001).
- ¹⁵ G. Cuniberti, M. Sassetti, and B. Kramer, Phys. Rev. B**57**, 1515 (1998); M. Vicari, A. Braggio, E.G. d'Agliano, and M. Sassetti, Eur. Phys. J. B**25**, 115 (2002).
- ¹⁶ R.G. Mani, J.H. Smet, K. Klitzing, V. Narayanamurti, W.B. Johnson, and V. Umansky, Nature (London) **420**, 646 (2002).
- ¹⁷ X.L. Lei and S.Y. Liu, Phys. Rev. Lett. **91**, 226805 (2003); J.C. Cao and X.L. Lei, Phys. Rev. B**67**, 85309 (2003).
- ¹⁸ B. Ferguson and X.C. Zhang, Nature Materials **1**, 26 (2002); Yu. P. Gousev, I. V. Altukhov, K. A. Korolev, V. P. Sinis, M. S. Kogan, E. E. Haller, M. A. Odnoblyudov, I. N. Yassievich, and K. A. Chao, Appl. Phys. Lett. **75**, 757 (1999).
- ¹⁹ Guanghui Zhou, Mou Yang, Xianbo Xiao, and Yuan Li, Phys. Rev. B**68**, 155309 (2003).
- ²⁰ D.F. Walls and G.J. Milburn, *Quantum Optics* (Springer-Verlag, Berlin, 1994).
- ²¹ F. Kassubek, C.A. Stafford and H. Grabert, Phys. Rev. B**59**, 7560 (1999); J.A. Torres and J.J. Saénz, cond-mat/0012250 (unpublished).
- ²² R. Landauer, Philos. Mag. **21**, 863 (1970); M. Büttiker, Phys. Rev. B**35**, 4123 (1987).
- ²³ In the resonant case of $\gamma = 0$, with the system parameters selected in this work $\xi = 5.5$. According to Eq. (6), $k_+ > 0$ requires that $E > \epsilon'_1 + \xi/2 = 2.52$.

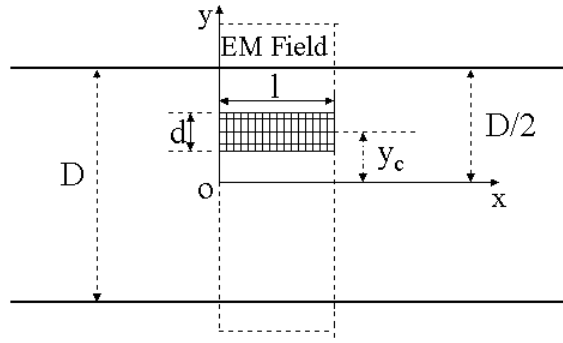


FIG. 1: Sketch of the system

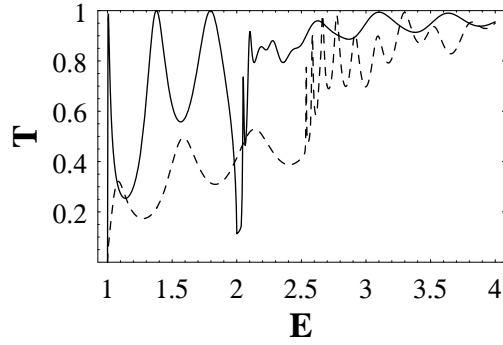


FIG. 2: Transmission probability T dependence on the incident energy E (in units of ϵ_1) for two combinations of the field parameters in the energy range (ϵ_1, ϵ_2) , the dashed line for $\omega = 3.57$ ($\gamma = 0$, resonant case) and $\epsilon = 9.96$, while the solid line for $\omega = 2$ and $\epsilon = 2.97$. We have used the parameters of $D = 200\text{\AA}$, $d = 0.1D$, $l = 25$ and $y_c = 0.17D$ such that $\epsilon'_1 = -0.23$ and $\epsilon'_2 = 3.34$.

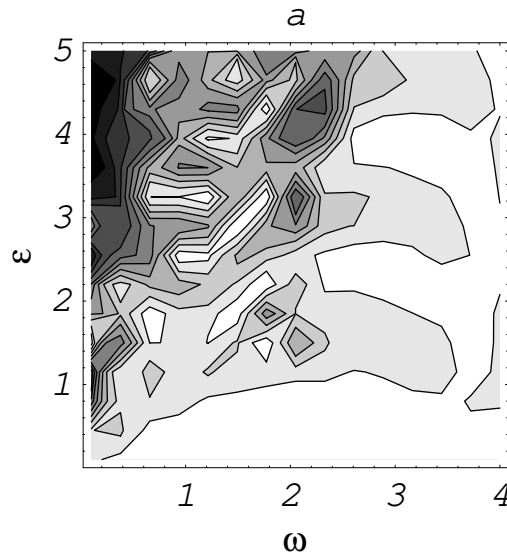


FIG. 3: Transmission probability T dependence on both field frequency ω and amplitude ϵ with incident energy $E = 2$, the system parameters are the same as in Fig. 2.

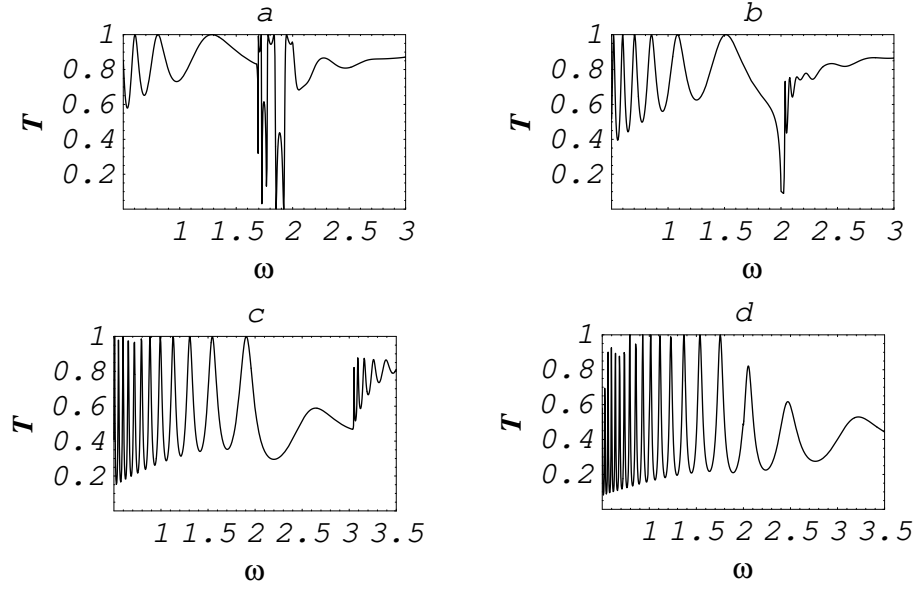


FIG. 4: Transmission probability T dependence on field frequency ω with incident energy $E = 2$ for serval field amplitudes: (a) $\varepsilon = 1.5$, (b) $\varepsilon = 2.97$, (c) $\varepsilon = 6$ and (d) $\varepsilon = 10$. The system parameters are the same as in Fig. 2.

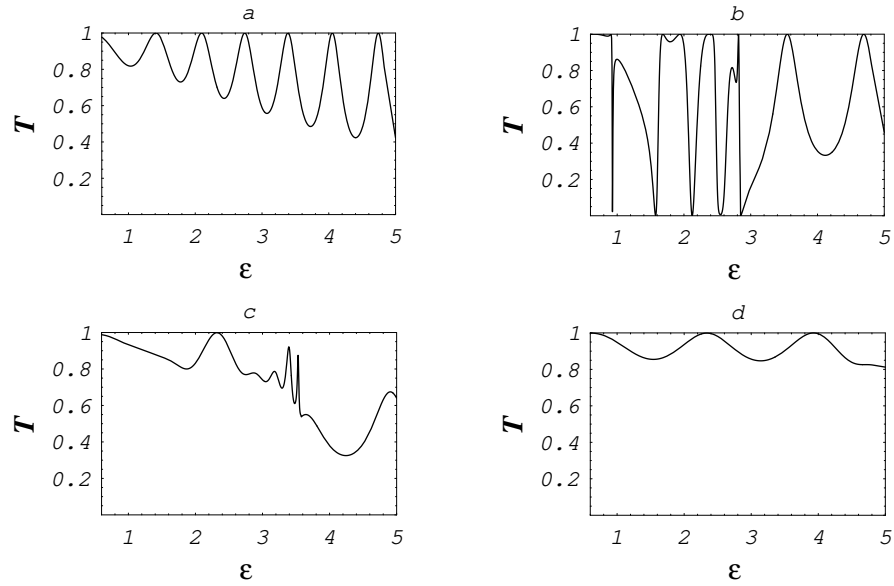


FIG. 5: Transmission probability T dependence on field amplitude ε with incident energy $E = 2$ for serval frequency: (a) $\omega = 1$, (b) $\omega = 2$, (c) $\omega = 2.3$ and (d) $\omega = 4$. The system parameters are the same as in Fig. 2.

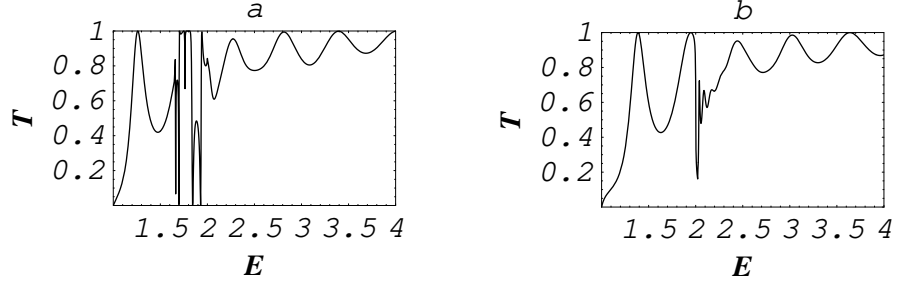


FIG. 6: Transmission probability T dependence on incident energy E for a different impurity width of $d = 0.2D$ with field frequency $\omega = 2$: (a) $\varepsilon = 2.97$ and (b) $\varepsilon = 3.6$. With the same length l and strength v as in Fig. 2 the change of the impurity width induces $\epsilon'_1 = -1.85$ and $\epsilon'_2 = 3.19$

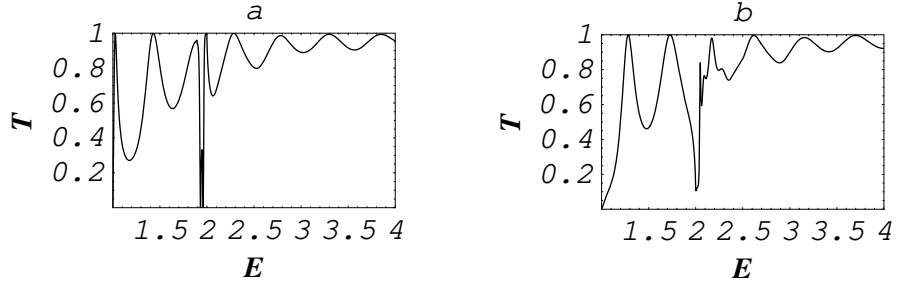


FIG. 7: Transmission probability T dependence on incident energy E for a different impurity strength of $v = -8$ with field frequency $\omega = 2$: (a) $\varepsilon = 2.97$ and (b) $\varepsilon = 3.2$. In this case $\epsilon'_1 = -0.64$ and $\epsilon'_2 = 3.26$ with the same impurity size as in Fig. 2.